NUCLEI AND NUCLEAR REACTIONS

STUDY OF ANGULAR DISTRIBUTION AND KNO SCALING IN THE COLLISIONS OF ^{28}Si WITH EMULSION NUCLEI AT 14.6A GeV

M. AYAZ AHMAD,[1] SHAFIQ AHMAD[2]

[1]**Physics Department, Faculty of Sciences, Tabuk University**
(P.O. Box 741, Saudi Arabia, K.S.A.; e-mail: mayaz.alig@gmail.com)

[2]**Physics Department, Aligarh Muslim University**
(Aligarh, 202002, India; e-mail: sahmad2004amu@yahoo.co.in)

An attempt has been made to study the angular characteristics of heavy ion collision at high energy in the interactions of ^{28}Si nuclei using with nuclear emulsion. The KNO scaling behavior in terms of the multiplicity distribution has been studied. A simplest universal function has been used to represent the present experimental data.

1. Introduction

The advent of heavy-ion collisions at relativistic energies has obtainable mission to explore new avenues in the field of high-energy physics. With the availability of heavy-ion beams at high energies, it has become possible to detect the existence of the phase transition from hadronic matter to Quark-Gluon Plasma (QGP) in a laboratory. It has been suggested that the strongly interacting matter at a high temperature of the order of 200 MeV ($\sim 10^{12}$ K) and the energy density of the order of 3 GeV/fm^3 produced in these collisions may undergo a phase transition to QGP [1, 2]. Such a phase transition could produce large fluctuations in the phase space apart from other possible signatures of the QGP formation, which includes the photon production, strangeness enhancement, J/ψ suppression, di-lepton production, fluctuations, and correlations. At present, most of the studies carried out have focused attention primarily on the search for a quark-gluon plasma, which might have be formed in such collisions. However, a number of other interesting aspects can give a vital information about the mechanism of particle production in heavy ion collisions. It is easy to visualize that the angular distribu-

tion, pseudorapidity distribution, and multiplicity distribution of hadrons produced in high-energy particle collisions are regarded as sources of information about the underlying production processes. Various models have predicted the multiplicity distribution of hadrons in hadron-hadron and hadron-nucleus collisions. The Koba–Nielsen–Olesen scaling hypothesis [3] known as the KNO scaling has become the dominant framework to study experimentally [4] and theoretically [5] the behavior of the multiplicity distribution of relativistic secondary hadrons produced in high-energy collisions. It will be of interest to apply the KNO scaling to nucleus-nucleus collisions at high energies for relativistic shower particles, slow and fast target-associated protons produced in the interactions of ^{28}Si nuclei with a nuclear emulsion.

In the present paper, we have reported on our experimental results, which include the angular distributions, pseudorapidity distributions of produced charged particles, rapidity gap distribution, and multiplicity distributions of relativistic shower, grey, and black particles produced in terms of the KNO scaling in the interactions of ^{28}Si nuclei with a nuclear emulsion at 14.6A GeV. A simplified universal function has been used to represent the experimental data.

2. Experimental Details

In the present study, two stacks of the *FUJI*-type emulsion, which has a printed grid on the air-surface and was exposed horizontally to a 14.6A GeV silicon beam at the Alternating Gradient Synchrophasotron (AGS)
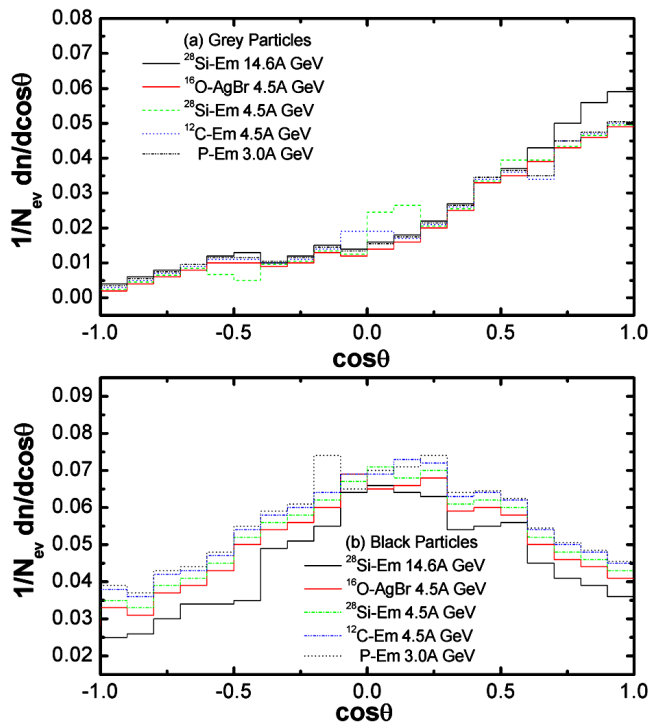
Fig. 1. (*a* and *b*) Angular distribution of charged secondaries produced in various interactions at high energies

of Brookhaven National Laboratory (BNL, New York, USA), have been utilized for the data collection. The dimensions of stacks used are the order of $16 \times 10 \times 0.06$ cm^3, and the quality of a beam in terms of the incident beam flux is the order of $\sim 3.0 \times 10^3$ ions/cm^2. The method of line scanning has been adopted to scan the stacks, which was carried out carefully, by using NIKON (LABOPHOT and Tc-BIOPHOT, Japan) high-resolution microscopes with a 8 cm movable stage using 40X objectives and 10X eyepieces by two independent observers, so that the bias in the detection, counting, and measurements can be minimized. The interactions due to beam tracks making an angle $< 2°$ to the mean direction and lying in the emulsion at depths > 35 μm from either surface of the pellicles were included in the final statistics. The emulsion stacks used in the present experiment have density ρ of $\sim$ 3.60 g/cm^3 for Fuji ET 7B. A collection of 1205 events at the ^{28}Si-emulsion interaction at 14.6A GeV was picked up by following 141.59 m of the primary track length. This leads to the mean free path $\lambda_{\text{ine}} = (11.75 \pm 0.34)$ cm. The other relevant details of the present experiments and the target identifications can be seen in our earlier publications [6, 7].

3. Results and Discussions

Based on the above experimental background, we have obtained the following results.

3.1. Angular distribution of slow and relativistic particles

3.1.1 Angular distribution of slow particles

The angular distribution of target fragments, i.e. grey and black particles produced in the ^{28}Si-Em interactions at 14.6A GeV, ^{28}Si-Em and ^{12}C-Em at 4.5A GeV, respectively, are shown in Fig. 1 (*a* and *b*). In order to compare these distributions, the results due to α-Em collisions at 4.5A GeV [8] and the P-Em interactions at 3.0 GeV [9] are also given in the same figure. From these figures, one may notice that both these distributions are independent of the mass of beam nuclei. Moreover we note that no peculiarity or bump structure is observed, which may indicate the occurrence of nuclear shock wave phenomenon and/or any abnormal phenomenon. The forward and backward hemispheres are defined as the regions, where the emission angles are less than $90°(\theta < 90°)$ and greater than $90°(\theta > 90°)$, respectively. The forward $(\theta < 90°)$ to backward $(\theta > 90°)$ ratio for these distributions are calculated and presented in Table 1. A weak dependence of the forward/backward (F/B) ratio on the mass of the projectile is observed in the distributions of target fragments, which show an increase in the collisions impact with the mass of projectiles. It may be further concluded that black tracks are emitted nearly isotropically in the laboratory system. A slight increase in the forward direction is observed, whereas grey tracks are emitted largely in the forward direction.

3.1.2 Angular distribution of relativistic charged particles

The angular distributions of shower particles produced during the ^{28}Si-Em collisions at 14.6A GeV along with

T a b l e 1. Values of the forward/backward ratio of angular distributions of the produced particles in nuclear collisions

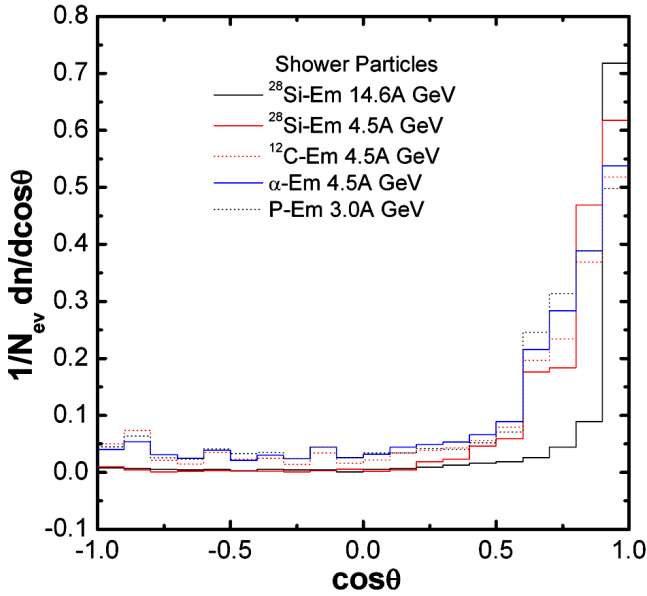| Projectile	Energy (A GeV)	Shower	Grey	Black
^{28}Si Present	14.6	18.06 ± 0.57	4.78 ± 0.21	1.37 ± 0.09
^{28}Si Ref. [10]	4.5	39.08 ± 2.39	5.29 ± 0.24	1.84 ± 0.06
^{12}C Ref. [10]	4.5	38.93 ± 3.21	4.69 ± 0.18	1.49 ± 0.04
^{4}He Ref. [11]	4.5	11.50 ± 0.66	3.00 ± 0.10	1.42 ± 0.04
P Ref. [11]	3.0	10.51 ± 1.40	3.36 ± 0.20	1.30 ± 0.05

Fig. 2. Angular distribution of shower particles produced in various interactions at different energies

Fig. 3. Pseudorapidity distribution of the shower particles produced at various energies and a red one for the present data

the data obtained by other workers [10–12] at $4.5A$ GeV in the ^{28}Si-Em, ^{12}C-Em, α-Em, and P-Em interactions, respectively, are shown in Fig. 2. It can be seen from the figure that the angular distributions of relativistic hadrons are almost similar, and the prominent peaks are observed at smaller angles. These peaks can be attributed to the surviving fragment of the projectile nucleus with the fragment charge $Z = 1$ superimposed on the uniform distribution.

Furthermore, we have calculated the forward/backward ratio for the relativistic shower charged particles, which is given in Table 1. A strong dependence of F/B in case of relativistic charged secondaries shows that these are closely associated with projectile nucleons.

3.2. Pseudorapidity distribution

The single-particle pseudorapidity distribution is one of the basic tools to study the angular characteristics of heavy ion collisions at high energies. It can provide us with the substantial information about the geometry and the dynamics of collisions. The pseudorapidity, η, of a particle is calculated by the relation $\eta = -\ln \tan(\theta_{\mathrm{S}}/2)$, where θ_{S} is the space angle of produced particles with respect to the mean direction of a beam.

Figure 3 shows the normalized pseudorapidity distributions (i.e. the particle number densities in the rapidity space) of the secondary charged shower particles emit-
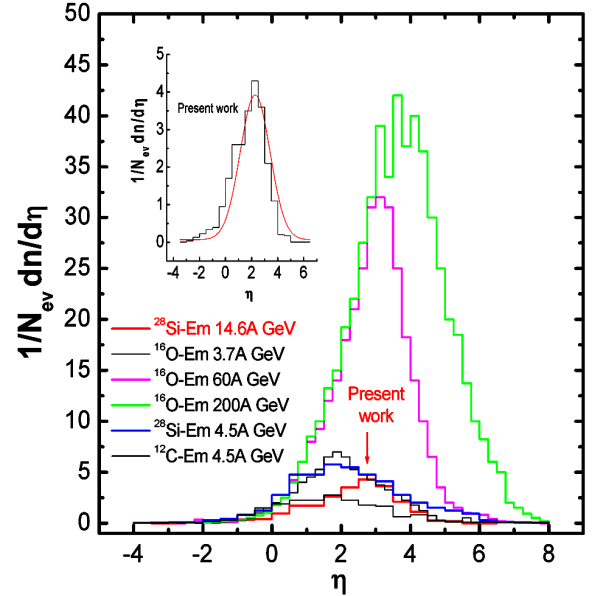
ted in the ^{28}Si-Em interactions at $14.6A$ GeV. In the same figure, the results obtained from the ^{28}Si-Em and ^{12}C-Em interactions at $4.5A$ GeV [12] along with the result concerning the ^{16}O-AgBr interaction at 3.7, 60, and $200A$ GeV [13], respectively, have been shown for comparison. One may notice that the η-distributions are completely scaled in the region of smaller values of η and also found to be independent of the mass of incident beam particles, whereas a weak energy dependence has been found in this region. The distribution is broader for a higher mass and the beam energy. The height of the centroid increases many times in the case of nucleus-nucleus collisions with respect to the proton-nucleus collisions [8].

The variation of the probability distributions of relativistic charged shower particles produced per unit rapidity, $P(N_{\mathrm{S}}, \eta) = (1/N_{\mathrm{S}})\,(dn/d\eta)$, with pseudorapidity, η, have been shown in Fig. 4 for the ^{28}Si-Em collisions at $14.6A$ GeV along with the ^{28}Si-Em, ^{12}C-Em, and P-Em collisions at $4.5A$ GeV, respectively. The distributions are normalized to the total number of hadrons produced in each sample. From this figure, one may notice that the distributions are almost completely scaled for the entire region of η except for large η-values, where a mild projectile dependence is seen. It may further be marked that the position and the height of the centroid remains the same in all cases. Thus, one may conclude that the multiparticle production at all angles in the laboratory
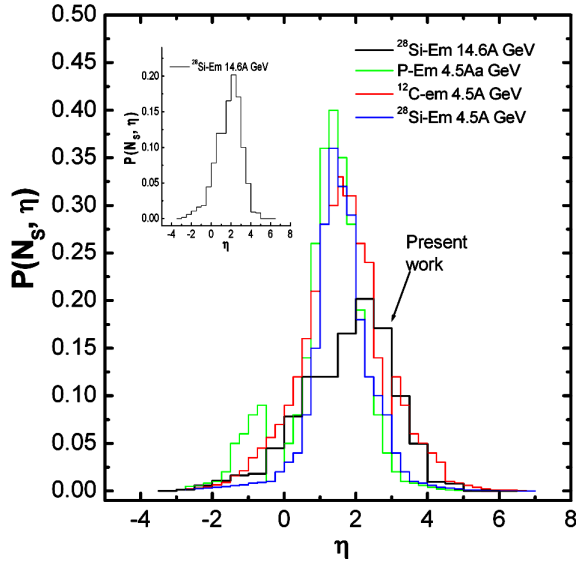
Fig. 4. Variation of the probability distribution of hadrons produced in various interactions at high energies

Fig. 5. Two-particle rapidity gap distribution in the ^{28}Si-Em interaction at 14.6A GeV

frame is the same in nucleus-nucleus and hadron-nucleus collisions at different projectile energies.

3.2.1 Rapidity gap distribution

The study of the correlation behavior amongst the relativistic particles helps one to investigate the mechanism of multiparticle production in high-energy heavy ion collisions. This is achieved by examining the correlations for various rapidity intervals. The occurrence of clustering amongst charged secondary particles would convincingly reveal that the secondary particles emitted in the hadronic interaction at high energies arise through the decay of clusters. The rapidity gap is defined as the difference in the rapidities between neighbouring final-state particles, when the pseudorapidities, $\eta, (= -\ln\tan(\theta_{S}/2))$, where θ_{S} is the space angle of shower particles with respect to projectile) of all the charged particles in each interaction are arranged in the increasing order $(\eta_1 < \eta_2 < \eta_3 < \ldots.\eta_n)$. The difference $\eta_{i+1} - \eta_i$ is known as a two-particle rapidity gap, where i can have values $1, 2, 3, \ldots, n-1$. Similarly, $\eta_{i+2} - \eta_i$ gives the three-particle rapidity gap, where $i = 1, 2, 3, \ldots, n-2$, and so on. In order to eliminate the contribution due to the diffraction dissociation, the secondary particles on each end of the rapidity space have been excluded from the analysis, because they are leading and target particles.

Figure 5 depicts the two-particle rapidity gap distributions of relativistic shower particles produced in ^{28}Si-

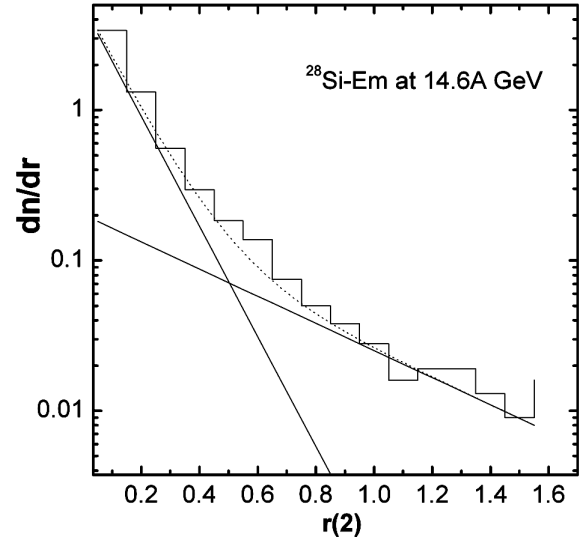emulsion collisions at 14.6A GeV. The presence of sharp peaks at relatively smaller values of rapidity gaps (r) in the above distributions provides the convincing evidence in support of the existence of short-range correlations, which reveals, in turn, that the relativistic particles are produced through the formation and the decay of clusters [14]. Similar results have been reported in hadron-hadron, hadron-nucleus, and nucleus-nucleus at different energies [14, 15]. The rapidity gap distribution at high energies can be well represented by a two-channel generalization of the Chew–Pignotti model [16] of the form

$$dn/dr = A \exp(-Br) + C \exp(-Dr). \qquad (1)$$

Here, dn/dr is the cluster density, and B denotes the correlation strength. The values of A, B, C, and D appearing in Eq. (1) are determined with the help of the CERN standard programme MINUIT, and the best fit equation for the ^{28}Si-Em data with χ^2/DF as 0.43 and 1.37 is given by

$$dn/dr = (4.39 \pm 0.07)\exp(-11.65r \pm 0.37)+$$

$$+(0.68 \pm 0.06)\exp(-2.53r \pm 0.058). \qquad (2)$$

The first term in Eq. (2) represents the short-range correlation and contributes significantly. The second term represents the long-range correlation and does not play any important role in the particle production. The continuous curves in the Fig. 5 represent Eq. (2), and the dashed lines give the individual contributions of the two

terms appearing in (2). It is evident from the figures that the maximum contribution to the correlation comes from the first term indicating a strong short-range correlation, while the contribution of the second term is quite small, giving the poor indication for the long-range correlation.

3.2.2 Cluster size

In order to find the cluster size in the pseudorapidity space, Adamovich *et al.* [17] have suggested the relations

$$dn/dr = \exp(-\rho\, mr) \quad \text{(for small } r\text{)}, \tag{3}$$

$$dn/dr = \exp(-\rho\, r) \quad \text{(for large } r\text{)}, \tag{4}$$

where ρ and m are, respectively, the cluster density and the cluster multiplicity defined as the number of charged shower particles in a cluster. The ratio B/D gives the value of m, which is found to be 4.61 and 5.10, respectively, for the ^{28}Si-Em data using Eq. (2). From the survey of the literature, it is noted that the values of m lie between 3 and 4 at different energies in hadron-hadron and hadron-nucleus collisions [17]. This shows that the cluster size is independent of the projectile energy and the type of interactions. The value of m in AA collisions is found to be more than that in hadron-hadron and hadron-nucleus collisions.

3.3. KNO Scaling in terms of multiplicity distributions

The study of multiplicity distributions of hadrons produced in high-energy particle collisions has been made extensively for hadron-hadron, hadron-nucleus and nucleus-nucleus interactions in the past, since such studies are useful in understanding the production processes involved. Koba, Nielsen, and Olesen [3] predicted that the multiplicity distributions of produced particles in a certain high-energy collision should exhibit a simple scaling law known as the KNO scaling, when expressed in terms of the scaling variable $Z(= N_i/\langle N_i\rangle)$, where N_i correspond to produced particles $N_{\rm S}$, $N_{\rm g}$, and $N_{\rm b}$. If $P_n(s)$ represents the probability for the production of n charged particles in an inelastic hadron-hadron collision, the multiplicity distribution in high-energy collisions at the center-of-mass energy $\sqrt{s}$ then exhibits a scaling law of the form

$$P_n(s) = \frac{\sigma_n(s)}{\sigma_{\rm inel}} = \frac{1}{\langle N\rangle}\Psi\left(\frac{N}{\langle N\rangle}\right) = 1/\langle N\rangle\Psi(z),$$
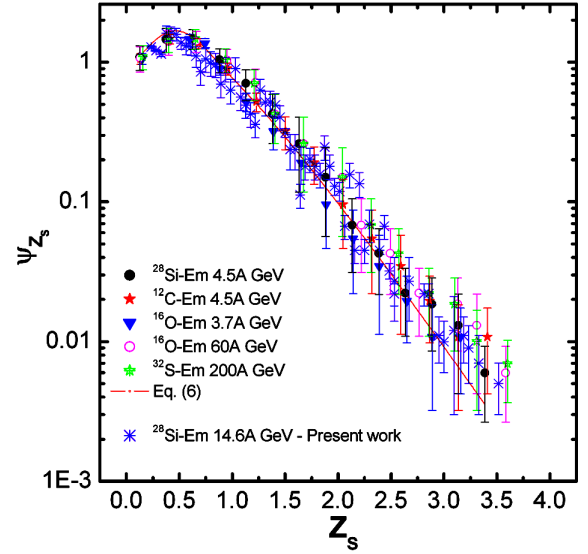
and

$$\sum P_n(s) = 1. \tag{5}$$

Fig. 6. Shower particle multiplicity distribution in terms of the KNO scaling for various interactions at different energies

Here, $\sigma_n(s)$ is the partial cross-section for the production of n charged particles, $\sigma_{\rm inel}$ is the total inelastic cross-section, and $\langle N\rangle$ is the average number of charged particles produced. The KNO scaling thus implies that the multiplicity distribution is universal, and $\Psi(Z)$ is an energy-independent function at sufficiently high energies, when expressed in terms of the scaling variable Z.

The other consequences of the KNO scaling are given as

(i) The normalized moments $C_k = \langle N^k\rangle/\langle N\rangle^k$ of the multiplicity distributions become independent of the projectile energy.

(ii) It leads to the relation $D/\langle N_{\rm S}\rangle = $ constant; provided $\Psi(Z)$ is not the delta function.

(iii) Central moments, $\sqrt[k]{\mu_k} = \sqrt[k]{(N - \langle N\rangle)^k}$, of the distribution should have a linear relation with the average multiplicity, $\langle n\rangle$, of the reaction.

It has been found by various researchers that the empirical expression for $\Psi(Z)$ in hadron-hadron and hadron-nucleus interactions obeys the semiinclusive KNO scaling, starting from few GeV. It is desirable to make similar studies of nucleus-nucleus collisions, as it is expected that nucleus-nucleus interactions at these energies can be visualized as a superposition of nucleon-nucleon collisions. In several works [18–20], it was reported that the validity of the KNO scaling holds for the projectile helium particle and target black fragments in heavy-ion interactions at the Dubna, Bevatron, CERN and AGS energies. It has been shown [20, 21] that the multiplicity distributions of secondary particles due to
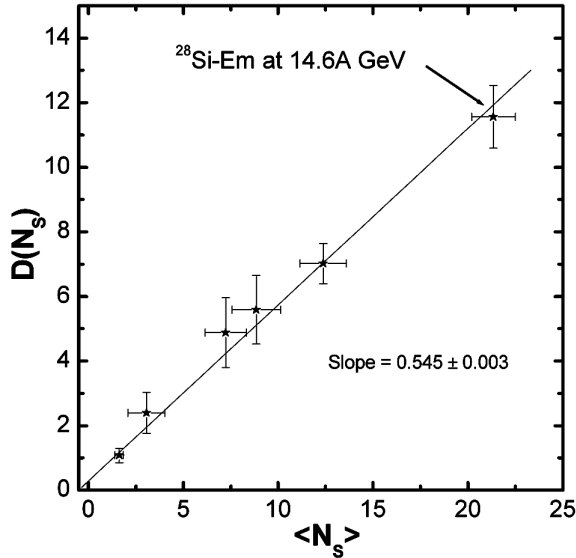
Fig. 7. Variation of the dispersion $D(N_S)$ as a function of $\langle N_S \rangle$ at various energies. Some experimental data are taken from [4, 8, 25, 26]

different projectiles in a wide range of energies in AA collisions can be represented by a universal function of the form

$$\Psi(z) = Az \exp(-Bz), \tag{6}$$

where A and B are constants.

In order to study the scaling behavior of shower particles produced in the ^{28}Si-Em collisions at 14.6A GeV, we have displayed the graph $\Psi(Z_S)$ as a function of Z_S in Fig. 6. The data points for the interaction of ^{28}Si and ^{12}C at 4.5A GeV, ^{16}O at 3.7A GeV and 60A GeV [18, 22], and ^{32}S at 200A GeV [23], respectively, with emulsion nuclei are also shown in the same figure. It is worth to note that relation (6) reproduces the shower particle multiplicity distribution well at different energies. One can see that the scaling in the form of relation (6) seems to qualitatively describe the trend of the multiplicity distribution of secondary particles produced in nucleus-nucleus collisions similar to that found in hadron-hadron and hadron-nucleus collisions. The values of constants A and B are determined with the help of the CERN standard programme MINUIT, and the best fit values of the parameters for the data used are $A = 11.004 \pm 0.038$ and $B = 2.23 \pm 0.076$, respectively, with $\chi^2/\mathrm{DF} = 0.131$, where DF means the degree of freedom. If the experimental points from the tail of the curve are not considered due to a low significance of experimental data, then χ^2/DF reduces to 0.081, which represents,

of course, a better fit and seems to confirm the validity of the universal scaling function. Further, it is investigated that the scaling violations are small, and the data exhibit KNO scaling within experimental errors.

The KNO scaling indicates that $\langle N_S \rangle$ should vary linearly with $\ln S$, which is also a consequence of the Feynman scaling [24]. To test the validity of the KNO scaling, the normalized moments, C_k, of multiplicity distributions are defined as

$$C_k = \langle N^k \rangle / \langle N \rangle^k \quad \text{for} \quad k = 2, 3, 4, \tag{7}$$

where $\langle N^k \rangle = \sum N^k \sigma_n / \sigma_{\mathrm{inel}}$, which should become independent of the projectile energy, if the multiplicity scaling is valid. The values of C_k-moments for $k = 2$ and 3 of shower particles produced in the interactions of ^{28}Si, ^{24}Mg, ^{14}N, and ^{12}C ions in the emulsion at various energies are presented in Table 2. It is clear that the values of C_2 and C_3 moments are found to be independent of the masses and the energy of the projectiles within the experimental errors. On the other hand, the higher moments corresponding to $k = 4, 5$ show an increasing trend in their values (not shown in Table 2), as the mass number of the projectile increases. The other consequence of the KNO scaling predicts that the central moments, $\sqrt[k]{\mu_k} = \sqrt[k]{\langle (N - \langle N \rangle)^k \rangle}$, of the distribution should have a linear relation with the average multiplicity $\langle N \rangle$ of the reaction, which leads to a generalization of the linear relation between the dispersion $D(N_S)$ and the average values of $\langle N_S \rangle$. The linear variation of $D(N_S)$ ($D = [\langle N_S^2 \rangle - \langle N_S \rangle^2]^{1/2}$) of shower particles as a function of $\langle N_S \rangle$ is illustrated in Fig. 7 for our data along with the other results [4, 8, 25, 26]. The best linear fit is represented by

$$D = \alpha + \beta \langle N_S \rangle \tag{8}$$

with a slope of (0.546 ± 0.004). The best straight line satisfies the data with reasonable confidence level and passes through the origin. The value of the slope in a similar case of proton-nucleus interactions reported by Gurtu $et\ al.$ [29] is (0.64 ± 0.02). It may be observed that the increase of the dispersion with $\langle N_S \rangle$ in the case of pp interactions [8] is slower than those for proton-nucleus and nucleus-nucleus collisions. This behavior indicates that some cascading within a nucleus takes place, which is not observed in pp interactions. The values of $\langle N_S \rangle / D$ for our data along with other results are also given in Table 2. An interesting observation can be seen from Table 2 that the values of
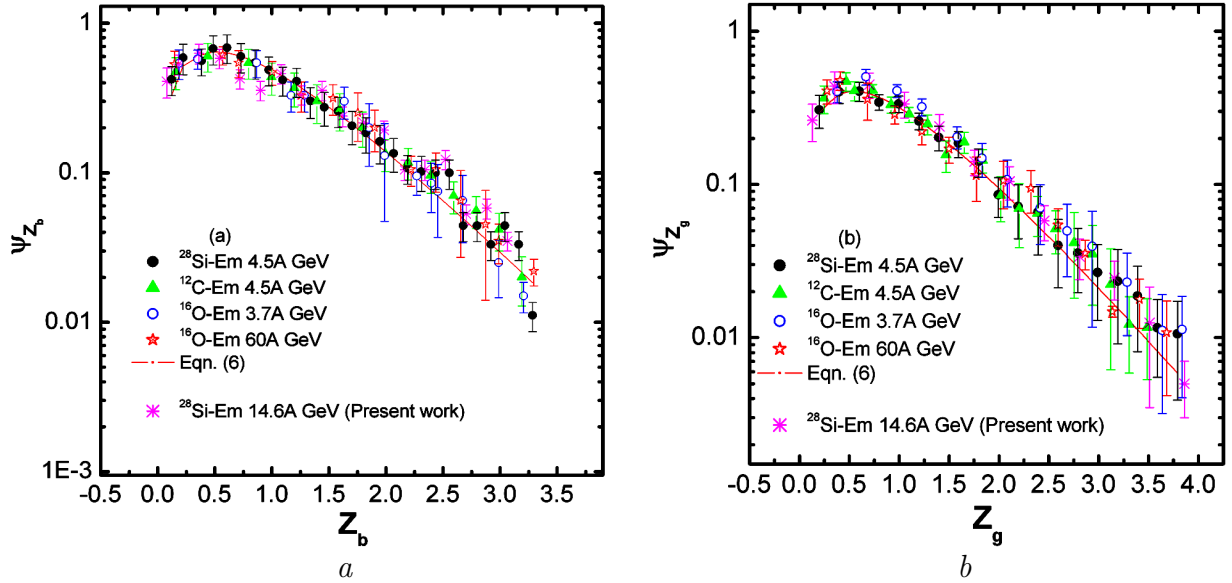
Fig. 8. a – Multiplicity distribution of slow target-associated protons in terms of the KNO scaling in the ^{28}Si-Em, ^{12}C-Em, and ^{16}O-Em interactions at 4.5, 3.7, and 60A GeV (the present work) at 14.6A GeV. b – Multiplicity distribution of fast target-associated protons in terms of the KNO scaling in the ^{28}Si-Em, ^{12}C-Em, and ^{16}O-Em interactions at 4.5, 3.7 and 60A GeV (the present work) at 14.6A GeV

T a b l e 2. **Values of $\langle N_{\rm S} \rangle$, $D(N_{\rm S})$, $\langle N_{\rm S} \rangle/D$ and the normalized moments for shower particles produced in various collisions**

Collisions (A GeV)	$\langle N_{\rm S} \rangle$	$D(N_{\rm S})$	$\langle N_{\rm S} \rangle/D(N_{\rm S})$	C_2	C_3	References
P-Em 4.5	1.63 ± 0.02	1.08 ± 0.02	1.51 ± 0.03	1.44 ± 0.02	2.55 ± 0.09	[27]
α-Em 2–10	3.06 ± 0.28	2.49 ± 0.04	1.23 ± 0.11	1.44 ± 0.04	2.55 ± 0.09	[8]
^{12}C-Em 4.5	7.24 ± 0.89	4.88 ± 0.38	1.48 ± 0.12	1.46 ± 0.01	2.66 ± 0.03	[12]
^{14}N-Em 2.1	8.85 ± 0.28	5.59 ± 0.17	1.58 ± 0.07	1.40 ± 0.05	2.58 ± 0.11	[25]
^{24}Mg-Em 4.5	12.37 ± 0.22	7.02 ± 0.02	1.76 ± 0.03	1.32 ± 0.08	2.11 ± 0.28	[19]
^{28}Si-Em 4.5	15.64 ± 1.23	11.91 ± 0.63	1.31 ± 0.07	1.57 ± 0.02	3.18 ± 0.13	[12]
^{28}Si-Em 4.5	15.32 ± 0.22	10.08 ± 0.22	1.52 ± 0.00	1.46 ± 0.11	2.81 ± 0.20	[28]
^{28}Si-Em 14.6	21.34 ± 0.15	11.56 ± 0.97	1.85 ± 0.16	1.29 ± 0.09	2.10 ± 0.02	Present work

$\langle N_{\rm S} \rangle/D$ for different projectiles and targets are approximately equal to those observed in hadron-nucleus interactions [29]. This feature may indicate that there is an essential similarity for the production mechanisms of two types of collisions. Furthermore, the agreement between hadron-nucleus and nucleus-nucleus collisions results suggests that $A - A$ collisions can be explained as a superposition of many nucleon-nucleon $(N - N)$ interactions, which is predicted by superposition models.

The multiplicity distributions of slow and fast target associated particles produced in ^{28}Si-emulsion collisions at 14.6A GeV have been investigated in the form of the KNO-scaling. A plot of $\Psi(z)$ as a function of the scaling variable $Z(= N/\langle N \rangle)$ for these medium-energy target-associated protons is shown in Figs. 8 (a and b). The

experimental points for ^{28}Si, ^{12}C at 4.5A GeV, ^{16}O at 3.7A GeV, and 60A GeV [22, 30], respectively, are also shown in the same figure. The solid curve in the figure is well represented by Eq. (6).

One can observe from the figures that the multiplicity distributions of slow and fast target-associated protons in nucleus-nucleus collisions at different energies are well described by Eq. (6) for different projectiles and seem to satisfy the scaling function. The best values of A and B are also found to be 11.00 ± 1.04, 2.14 ± 0.09 and 9.57 ± 1.09, 2.29 ± 0.09, respectively, for slow and fast target associated protons. The corresponding values of χ^2/DF are found to be 0.52 and 0.99, respectively, which indicates that the fitting is good for different projectiles at different energies in the case of slow protons, but a small deviation from the exact scaling can be seen for fast

target-associated protons in Fig. 8 (*b*). It is difficult to give any physical explanation of the multiplicity scaling for slow and fast protons, and, hence, it can be regarded as an empirical observation.

4. Conclusions

The present experimental study leads us to the following conclusions.

(*i*) The angular characteristics, i.e., the angular distributions of N_b, N_g, and N_S, and pseudorapidity distributions for shower particles, concluded the multiparticle production processes at all angles in the laboratory frame and are the same in nucleus-nucleus and hadron-nucleus collisions at different projectile energies.

(*ii*) Pseudo-rapidity distributions of relativistic shower particles produced are completely scaled in the region of smaller values of η, and the η distribution is found to be independent of the mass and the incident beam, whereas the weak energy dependence has been found in this region.

(*iii*) The multiplicity distributions of relativistic shower particles and slow and fast target-associated protons produced in the ^{28}Si-Em collisions at 14.6A GeV along with other experimental data at various energy ranges exhibit the KNO scaling within experimental errors, and small scaling violations are found. The values of normalized moments, C_2 and C_3, are found to be independent of the masses and the energies of the projectiles.

(*vi*) The observed features can be understood in terms of the geometry of collision processes.

1. M. Gazdzicki and S. Mrowczynski, Z. Phys. C **54**, 127 (1992); S. Mrowczynski, Phys. Lett. B**439**, 6 (1998).

2. M.A. Halasz, A.D. Jackson, R.E. Shrock, M.A. Stephanev, and J.J.M. Verbaarschot, Phys. Rev. D **58**, 96007(1998).

3. Z. Koba, H.B. Nielsen, and P. Olesen: Nucl. Phys. B **40**, 317 (1972).

4. P. Slattery, Phys. Rev. Lett. **29**, 1624 (1972).

5. W. Thane, K. Eggert, K. Giboni, H. Lisken, P. Darriulat, P. Dittmann, M. Holder, K.T. Mcdonald, H. Albrecht, T. Modis, K. Tittel, H. Preissner, P. Allen, I. Derado, V. Eckardt, H. J. Gebauer, R. Meinke, P. Seyboth, and S. Uhlig, Nucl. Phys. B **129**, 365 (1997).

6. S. Ahmad, M.A. Ahmad, M. Irfan, and M. Zafar, J. Phys. Soc. Japan **75**, 064604 (2006); M. Ayaz Ahmad, Shafiq Ahmad, and M. Zafar, Indian J. of Phys. **84**, 1675 (2010).

7. M. Ayaz Ahmad, *Ph.D. Thesis* (Aligarh Muslim University, Aligarh, 2010).

8. I. Otterlund, Nucl. Phys. B **142**, 445 (1978).

9. M. Bogdanski *et al.*, Helv. Phys. Acta **42**, 485 (1969).

10. M. Tariq, *Ph.D. Thesis* (Aligarh Muslim University, Aligarh, 1993).

11. A. Dabrowska *et al.*, Z. Phys. C **59**, 399 (1993).

12. M. Ayaz Ahmad, *M. Phil. Dissertation* (Aligarh Muslim University, Aligarh, 2005).

13. Zhang Dong-Hai *et al.*, Chin. Phys. Soc. **16**, 1009 (2007).

14. S. Roy, N.S. Arya, D.P. Goyal, A. Mozumder. P.K. Sengupta, and S. Singh, Phys. Rev. D **21**, 2497 (1980); J.B. Singh *et al.*, Phys. Rev. D **26**, 2479 (1982).

15. V.S. Shukla, K.B. Bhalla, A. Gill, V. Kumar, and S. Lokanathan, Int. J. Mod. Phys. A **3**, 1411 (1988).

16. G.F. Chew and A. Pignotti, Phys Rev. **176**, 2112 (1968).

17. M.I. Adamovich, M.M. Chernjavskii, I.M. Dremin, A.M. Gershkovich, S.P. Kharlamov, V.G. Larionova, M.I. Tretjakova, E.I. Volkov, and F.R. Yagudina, Nuovo Cim. A **33**, 183 (1976).

18. M. El-Nadi *et al.*, Nuovo Cim. A **108**, 831 (1995).

19. G. Singh, A.Z.M. Ismail, and P.L. Jain, Phys. Rev. C **43**, 2417 (1990); G. Singh, K. Sengupta, and P.L. Jain, Phys. Rev. C **42**, 1757 (1990); Phys. Lett. B **222**, 301 (1989).

20. Fu–Hu–Liu, Phys. Rev. C **62**, 024613 (2000).

21. M.M. Sherif, M.K. Hegab, A. Abdelsalam, S.A. El-Sharkawy, and M. Tawfik, Int. J. Mod. Phys. E **2**, 835 (1993).

22. M. El-Nadi *et al.*, Nuovo Cim. A **108**, 281 (1995); Nuovo Cim. A **108**, 87 (1995).

23. C.J. Waddington and P.S. Freier, Phys. Rev. C **31**, 888 (1985).

24. R.P. Feynman, Phys. Rev. Lett. **23**, 1415 (1969).

25. G.M. Chernov, K.G. Gulamov, U.G. Gulyamov, S.Z. Nasyrov, and L.N. Svechnikova, Nucl. Phys. A **280**, 478 (1977).

26. D. Ghosh, Amitabha Mukhopadhyay, Anit Ghosh, Ranjan Sengupta, and Jaya Roy, Nucl. Phys. A **499**, 850 (1989).

27. V.I. Bubnov *et al.*, Z. Phys. A **302**, 133 (1981).

28. B.K Singh, *Ph.D. Thesis* (Banaras Hindu Univ., Varanasi, 1995).

29. A. Gurtu, P.K. Malhotra, I.S. Mittra, P.M. Sood, S.C. Gupta, V.K. Gupta, G.L. Kaul, L.K. Mangotra, Y. Prakash, N.K. Rao, and M.K. Sharma, Phys. Lett. B **50**, 391 (1974).

30. N.N. Abd-Allah and N. Mohery, Turk. J. Phys. **25**, 109 (2001).

ВИВЧЕННЯ КУТОВОГО РОЗПОДІЛУ І КНО СКЕЙЛІНГУ В ЗІТКНЕННЯХ ^{28}Si З ЯДРАМИ ЕМУЛЬСІЇ ПРИ 14,6A ГеВ

М.А. Ахмад, Ш. Ахмад

Р е з ю м е

Досліджено кутові характеристики для зіткнень при високих енергіях важких іонів ^{28}Si з ядерною емульсією. Вивчено КНО (Коба–Нільсен–Олесен) скейлінг в термінах розподілу множинності. Для опису експериментальних даних використано просту універсальну функцію.